# Time-resolved structure-function coupling in brain networks

Zhen-Qi Liu[1,†], Bertha Vázquez-Rodríguez[1,†], R. Nathan Spreng[1],
Boris C. Bernhardt[1], Richard F. Betzel[2], Bratislav Misic[1*]

[1]*McConnell Brain Imaging Centre, Montréal Neurological Institute, McGill University, Montréal, Canada*
[2]*Psychological and Brain Sciences, Program in Neuroscience, Cognitive Science Program,*
*Network Science Institute, Indiana University, Bloomington, IN, USA*
†*These authors contributed equally to this work.*
(Dated: July 8, 2021)

The relationship between structural and functional connectivity in the brain is a key question in systems neuroscience. Modern accounts assume a single global structure-function relationship that persists over time. Here we show that structure-function coupling is dynamic and regionally heterogeneous. We use a temporal unwrapping procedure to identify moment-to-moment co-fluctuations in neural activity, and reconstruct time-resolved structure-function coupling patterns. We find that patterns of dynamic structure-function coupling are highly organized across the cortex. These patterns reflect cortical hierarchies, with stable coupling in unimodal and transmodal cortex, and dynamic coupling in intermediate regions, particularly in insular cortex (salience network) and frontal eye fields (dorsal attention network). Finally, we show that the variability of structure-function coupling is shaped by the distribution of connection lengths. The time-varying coupling of structural and functional connectivity points towards an informative feature of the brain that may reflect how cognitive functions are flexibly deployed and implemented.

## INTRODUCTION

The brain is a network of anatomically connected neuronal populations. Inter-regional signaling via electrical impulses manifests as patterns of organized co-activations, termed "functional connectivity". The coupling between structural connectivity (SC) and functional connectivity (FC) is a fundamental feature that reflects the integrity of neural signaling [5]. Historically, most studies have focused on static structure-function coupling over the course of a whole scanning session [73].

However, over the past decade functional connectivity is increasingly conceptualized as a dynamic process [46, 58, 71]. Functional connectivity patterns display time-resolved fluctuations that are non-random [10, 14, 26, 45, 84], highly organized [2, 28, 70, 80], individual-specific [40], related to behaviour [23, 34] and evolve over the lifespan [7]. As a result, structure-function coupling is also likely to fluctuate over multiple timescales. Indeed, multiple studies have reported evidence of dynamic structure-function relationships over the course of single recording sessions [30, 31], and over more protracted periods, including early childhood and young adult neurodevelopment [8, 35].

Importantly, previous studies on dynamic structure-function coupling worked under the assumption that structure-function relationships are uniform across the brain. Recent research suggests that structure-function coupling is regionally heterogeneous, such that structural and functional connectivity profiles are closely related in sensory (unimodal) cortex, but gradually decouple in transmodal cortex [8, 56, 59, 79]. The sys-

tematic decoupling or "untethering" of structure and function along this unimodal-transmodal gradient is thought to reflect differentiation in micro-architectural properties [12, 50, 73], including molecular, cellular and laminar differentiation [8, 36, 68, 79]. Indeed, computational models that implement regionally heterogeneous dynamics using micro-architectural properties make more accurate predictions of functional connectivity from structural connectivity [20, 21, 42, 82].

How do regional patterns of structure-function coupling fluctuate moment-to-moment? Here we derive time- and region-resolved patterns of structure-function coupling. We first estimate dynamic inter-regional co-fluctuation using a recently-developed temporal unwrapping method that does not require windowing [26, 28]. We then reconstruct dynamic patterns of regional structure-function coupling and contextualize these patterns with respect to macroscale brain organization, including intrinsic networks, as well as functional and cellular hierarchies.

## RESULTS

The results are organized as follows. We first reconstruct frame-by-frame co-fluctuation matrices from regional BOLD time-series [26, 28]. We then apply a multilinear model to estimate regional time-series of structure-function coupling [79], before comparing regional fluctuations in structure-function coupling with large-scale intrinsic networks [83], cortical hierarchies [48] and cytoarchitectonic classes [81]. We also benchmark the extent to which dynamic fluctuations in structure-function coupling can be explained by topological and geometric embedding. Finally, we assess the correspondence between conventional (static) structure-function coupling and dynamic structure-function cou-
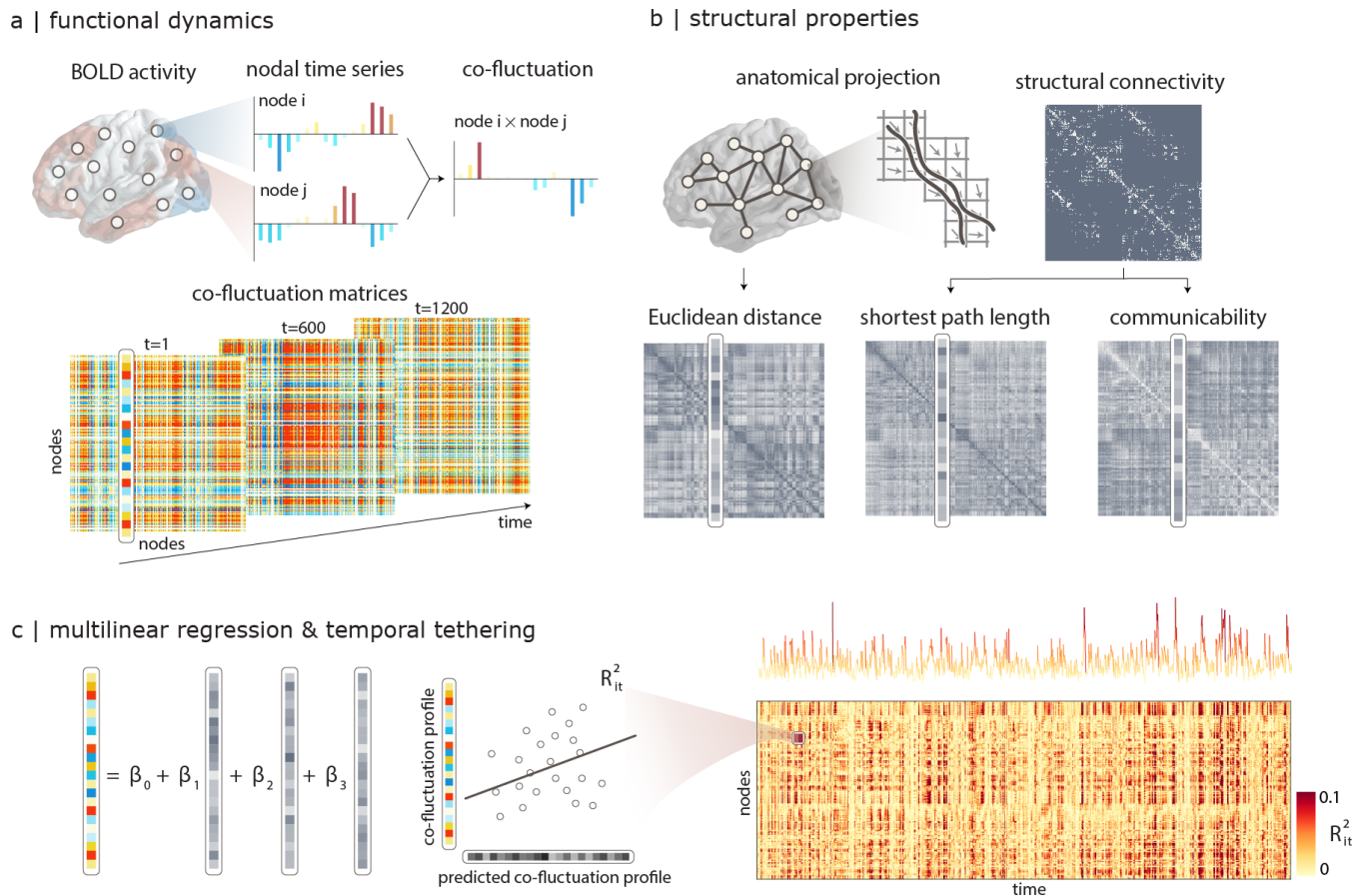
---

* bratislav.misic@mcgill.ca

**Figure 1 | Time-resolved structure-function coupling. (a)** The co-fluctuation of two brain regions $i$ and $j$ is calculated as the element-wise multiplication of the two z-scored fMRI BOLD activity time-series. The points of this time-series can be represented as one element in a co-fluctuation matrix. **(b)** Pairwise structural relationships are derived from structural connectivity networks reconstructed from diffusion MRI, including Euclidean distance between node centroids, shortest path length and communicability. **(c)** A multilinear regression model is used to predict a region's co-fluctuation profile from it's structural profile, using Euclidean distance, path length and communicability as predictors. The resulting coefficient of determination $(R_{i,t}^2)$ indicates how well structural profile predicts functional connectivity for a particular brain region $i$ at a particular time point $t$. The procedure generates a "temporal tethering" matrix that captures the fluctuation of structure-function coupling for individual regions across time. The time-series shows time-resolved fluctuations in mean $R^2$.

pling. Data were derived from $N = 327$ healthy, unrelated participants from the Human Connectome Project (HCP; [78]). Structural connectomes were reconstructed from diffusion MRI (dMRI). Static and dynamic functional connectivity were estimated from resting-state functional MRI (fMRI) (see *Materials and Methods* for detailed procedures). Analyses were performed using a network parcellation of 400 cortical nodes [63].

**Time-resolved structure-function coupling**

The temporal unwrapping procedure generates a node-by-node co-fluctuation matrix for each time point (Fig. 1a). We then use a multilinear regression model to predict the co-fluctuation profile of every node from its structural connectivity profile [33, 79]. The model

was fitted separately for each time point (Fig. 1c). Predictors in the model were three measures that quantify distinct types of communication [5, 65]: (1) Euclidean distance, (2) shortest path length, and (3) communicability (Fig. 1b). Euclidean distance embodies the notion that proximal neurons may exchange information more easily, and is consistent with navigation-like communication [66]. Shortest path length is a statistic that embodies centralized routing-like communication [29], while communicability is a statistic that embodies decentralized diffusion-like communication [17, 27]. All models were fitted independently for each individual participant.

The multilinear model allows us to quantify regional structure-function coupling across time. For each brain region $i$ and time point $t$, we measure the goodness of fit
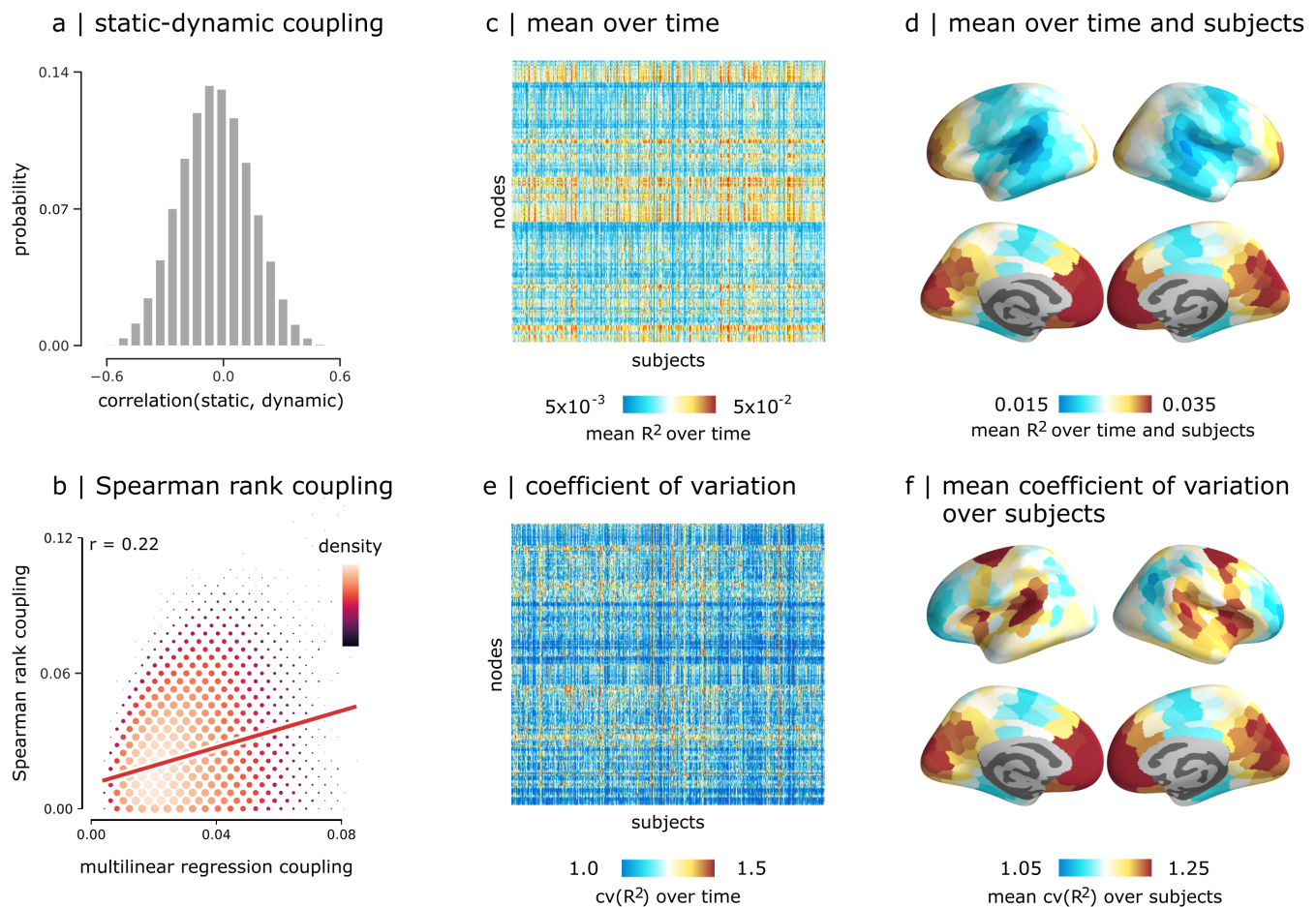
**a | static-dynamic coupling**

**c | mean over time**

**d | mean over time and subjects**

$5\times10^{-3}$ — $5\times10^{-2}$
mean $R^2$ over time

0.015 — 0.035
mean $R^2$ over time and subjects

**b | Spearman rank coupling**

r = 0.22

density

**e | coefficient of variation**

**f | mean coefficient of variation over subjects**

1.0 — 1.5
cv($R^2$) over time

1.05 — 1.25
mean cv($R^2$) over subjects

Figure 2 | **Dynamic structure-function coupling.** **(a)** Correlations between regional patterns of static and dynamic structure-function coupling. **(b)** Correlations between dynamic structure-function coupling estimated using a multilinear model [79] versus coupling estimated using an alternative Spearman rank correlation method [8]. **(c)** Mean time-resolved structure-function coupling over time. **(d)** Mean time-resolved structure-function coupling over time and subjects. **(e)** Coefficient of variation of structure-function coupling across time. **(f)** Coefficient of variation of structure-function coupling across time and mean over subjects.

using the coefficient of determination $R^2_{i,t}$ between the predicted and the empirical functional profile (Fig. 1c). A value near 1 indicates strong coupling between the structural and functional profiles for the $i$-th node at time $t$. These coefficients of determination are then assembled into a node × time structure-function coupling ("temporal tethering") matrix. The procedure was carried out separately for each individual in the sample.

Fig. 2a shows the Pearson correlations between dynamic structure-function coupling maps and the static structure-function coupling map reconstructed using the whole time-series. The coefficients span a wide distribution, encompassing both positive and negative values, suggesting that dynamic structure-function coupling provides a fundamentally different perspective on structure-function relationships. Fig. 2b shows the relationship between two alternative methods for estimating regional structure-function coupling. The abscissa shows

structure-function coupling values estimated using the multilinear model described above, while the ordinate shows the same values estimated using the method described by Baum and colleagues [8]. The latter, which we term "Spearman rank coupling", estimates structure-function coupling as the Spearman rank correlation between the structural and functional profiles of each node. The principal strength of the method is that it does not make arbitrary assumptions about which predictors to include; the principal weakness is that the correlation can only be computed between pairs of regions that have an underlying structural connection, potentially missing out on biologically-important dyadic relationships. Importantly, the two methods are positively correlated ($r = 0.22$), suggesting that similar conclusions about structure-function coupling can be drawn using the two methods.

Figs. 2c,d show the mean structure-function coupling

$R^2$, while Fig. S1 shows the contribution of individual predictors. To quantify the variability of structure-function coupling across time, we compute — separately for each participant — the coefficient of variation of $R^2$ across time ($\mathrm{cv}(R^2)$). The coefficient of variation is the ratio of the standard deviation of $R^2$ to the mean of $R^2$. It is a standardized measure of dispersion of $R^2$ values about the mean that captures the variability in structure-function coupling across time. In other words, $\mathrm{cv}(R^2)$ allows us to compare the variability of structure-function coupling time-series that have different means. Figs. 2e,f show that $\mathrm{cv}(R^2)$ is regionally heterogeneous and appears to be greatest in insular cortex, frontal eye fields, medial prefrontal and medial occipital cortex. In the following section, we analyze this pattern in greater detail.

### Hierarchical organization of dynamic structure-function coupling

We next consider how patterns of dynamic structure-function coupling reflect different features of cortical organization. Specifically, we focus on 3 widely studied cortical annotations, including the unimodal-transmodal principal functional gradient [48], intrinsic functional networks [63] and cytoarchitectonic classes [81]. In each case, we compute the mean coefficient of variation of structure-function coupling. Fig. 3b shows exemplar time-series of structure-function coupling for nodes in insular and parietal cortex, exhibiting distinct variability patterns. Figs. 3c-e show that brain regions that occupy intermediate positions in the cortical hierarchy tend to display the most dynamic fluctuations in structure-function coupling. Specifically, we find the most variable fluctuations in the middle of the unimodal transmodal hierarchy (classes 4-6), corresponding to the ventral attention/salience network and the insular cortex in the Yeo and Von Economo atlases, respectively, as well as the frontal eye fields, corresponding to the dorsal attention network. These observations are confirmed using spatial autocorrelation-preserving null models to test the null hypothesis that $\mathrm{cv}(R^2)$ is greater than expected in intermediate positions of the unimodal-transmodal hierarchy (Fig. S2). Altogether, the results show that structure-function coupling has an inverted U-shape relationship with cortical hierarchies. Namely, the insular cortex and frontal eye fields, intermediate in the unimodal-transmodal hierarchy, have the most variable structure-function coupling, while unimodal and transmodal cortex have more stable structure-function coupling.

### Relating static and dynamic structure-function coupling

In the previous section we considered how structure-function coupling fluctuates around the mean. We next ask: how closely do dynamic patterns of structure-function coupling reflect static structure-function coupling? To address this question, we systematically compare the dynamic an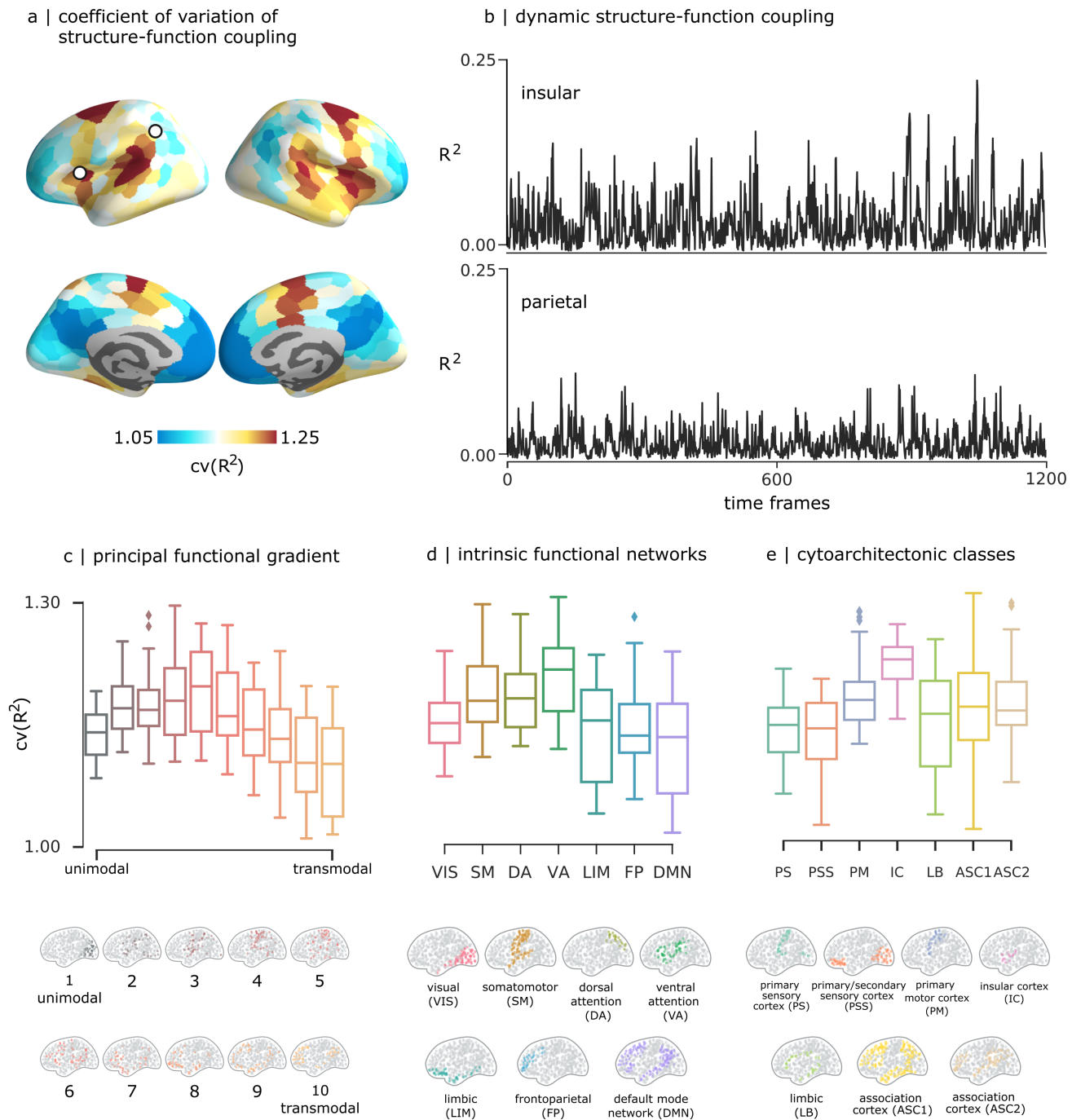d static case. Taking into account all time points in the dynamic case, we compute (a) the proportion of time points for which dynamic coupling is greater than static coupling ("dynamic > static"), (b) how similar the dynamic patterns are to the static pattern ("bias") and, (c) how tightly scattered the dynamic patterns are relative to the static pattern ("variance") (Fig. 4a).

We again observe a U-shape relationship with cortical hierarchies. In particular, we find that regions intermediate in the unimodal-transmodal hierarchy, corresponding to the insular cortex, tend to have greater dynamic than static coupling (Fig. 4b). These regions also have the closest correspondence between dynamic and static coupling (Fig. 4c) and the lowest dynamical variance around the static case (Fig. 4d). Altogether, these results suggest that the relationship between dynamic and static coupling is not uniform across the brain, but strongly depends on the region's position in the putative unimodal-transmodal hierarchy, with the closest correspondence between static and dynamic coupling observed in the middle of the hierarchy. Taken together with the results from the previous section, we reveal an interesting property about areas that are intermediate in the hierarchy, such as insular cortex and frontal eye fields. Namely, intermediate areas display the greatest overall fluctuations relative to the mean, but over time tend to follow and converge with static coupling.

### Spatial and topological determinants of dynamic structure-function coupling

We finally seek to understand how dynamic local structure-function coupling depends on geometric, anatomical and functional embedding. Given that the unimodal-transmodal hierarchy possibly reflects a continuous gradient of connection lengths [54, 55, 67], we ask whether dynamic structure-function coupling also reflects the distribution of connection lengths that a region participates in. Fig. 5a shows the map of mean connectivity distance for each region [54, 55]. These regional differences follow an inverted U-shape relationship with dynamic structure-function coupling, such that areas with very short and very long connection lengths tend to have more stable coupling, and areas with intermediate connection lengths tend to have more variable coupling. Fig. 5b shows that dynamic structure-function coupling is poorly correlated with multiple measures of structural and functional network embedding, including betweenness, clustering and degree. Altogether, these results suggest that the dynamic nature of structure-function coupling in "middle hierarchy" regions potentially originates from their connection length distribution.

Interestingly, when we compute the group-average similarity of inter-regional structure-function time-courses (i.e. how similar are inter-regional fluctuations in structure-function coupling), we find a comparable relationship with Euclidean distance (Fig. 5d). Namely, regions that are physically close together and far apart
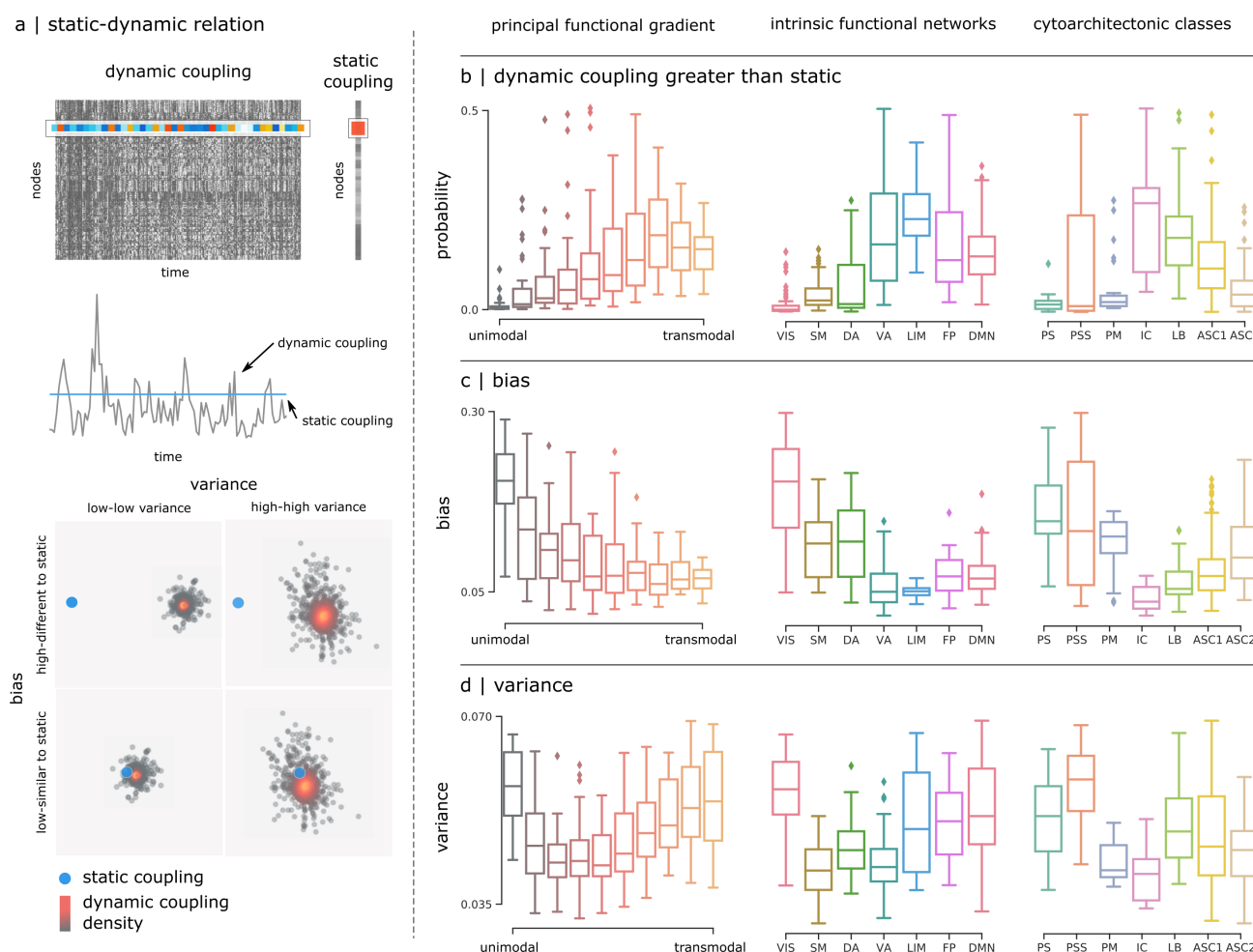
Figure 3 | **Relationship with cortical hierarchies. (a)** Coefficient of variation of the structure-function coupling, averaged over all participants. **(b)** Time-series of regional structure-function coupling shown for one region in parietal cortex (left) and one region in insular cortex (right) from one randomly selected participant. The mean coefficient of variation is displayed for three types of cortical annotations: **(c)** 10 equally-sized bins of the principal functional gradient [48], **(d)** intrinsic functional networks [83], and **(e)** von Economo cytoarchitectonic classes [81].

Figure 4 | **Relating static and dynamic structure-function coupling. (a)** Top: static structure-function coupling is estimated using the functional connectivity matrix derived from the whole resting-state time-series [79], and compared with dynamic coupling. The dynamic structure-function coupling of node $i$ corresponds to the $i^{th}$ row of the dynamic coupling matrix, while the static coupling corresponds to the $i^{th}$ element of static coupling vector. Middle: dynamic values represented as a time-series (black line) that fluctuates around the single static coupling value (blue line). Bottom: dynamic coupling values are represented as a scattered distribution of points (black) around the static coupling value (blue point). The two are compared in different cortical annotations using three summary statistics: **(b)** the probability of having a larger dynamic coupling value compared to the static coupling, **(c)** the bias, and **(d)** the variance of the dynamic coupling to reproduce the static values.
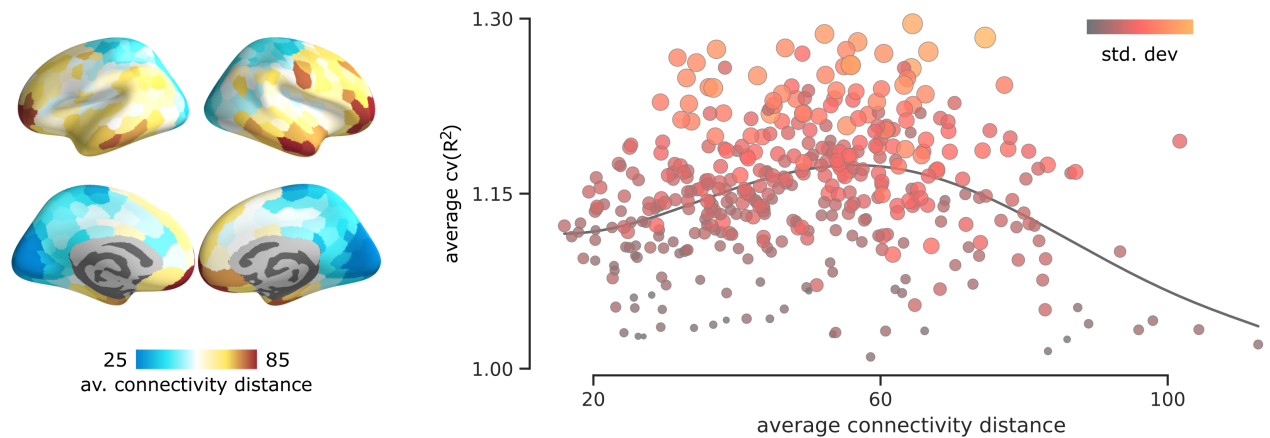
tend to display similar fluctuations in structure-function coupling, and regions that are at intermediate distances from one another tend to display dissimilar fluctuations in coupling. Finally, we compare the similarity of structure-function coupling between regions with the structural and functional connectivity between those regions. We find that the mean similarity of structure-function coupling is greater for areas that are structurally connected than areas that are not (t(79798) = 80.95, p < 0.001) (Fig. 5e). Likewise, mean similarity of structure-function coupling is greater for areas that participate in the same intrinsic networks than those that are in different networks (t(79798) = 45.34, p < 0.001)

(Fig. 5e). In other words, coordinated patterns of dynamic structure-function coupling are — as expected — driven by inter-regional structural and functional connectivity.
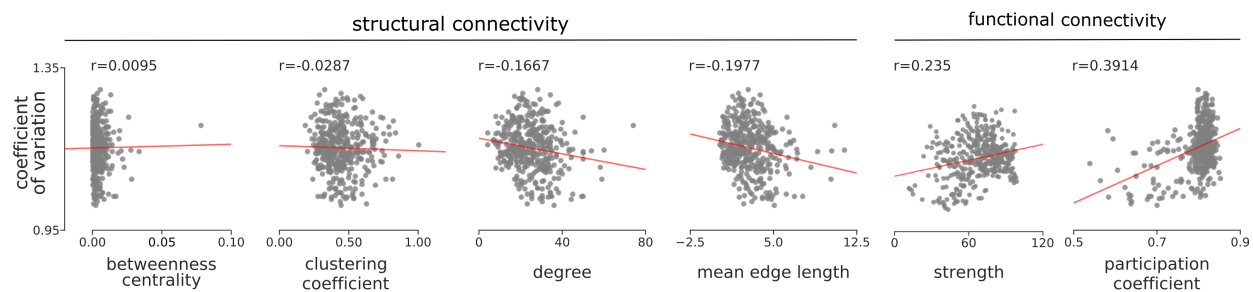
## DISCUSSION

Emerging theories emphasize dynamic functional interactions that unfold over structural brain networks [46]. Here we study time- and region-resolved patterns of structure-function coupling. We find that dynamic coupling patterns reflect cortical hierarchies, with the most dynamic fluctuations in the insula and frontal eye
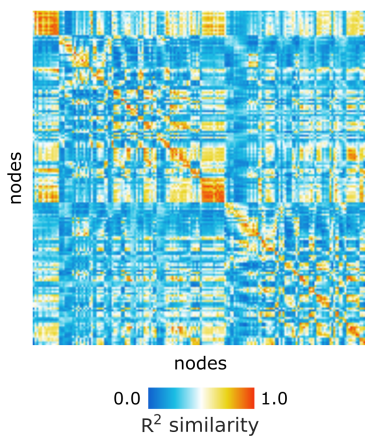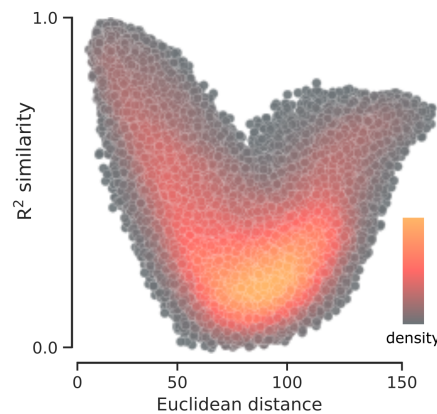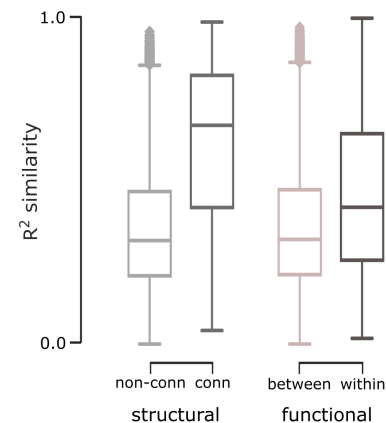
Figure 5 | **Spatial and topological determinants of structure-function coupling variability.** **(a)** Average connectivity distance calculated following [54], and correlated with the average coefficient of variation of the structure-function coupling from Fig. 3a. Scatter color and size represent the standard deviation. **(b)** Coefficient of variation of structure-function coupling compared to network embedding metrics derived from structural and functional networks. **(c)** $R^2$ similarity between pairs of nodes calculated as the Pearson correlation between pairs of regional structure-function coupling averaged across subjects **(d)** $R^2$ similarity correlated with Euclidean distance. Colormap show the density of the scatter plot. **(e)** $R^2$ similarity values grouped by structural connectedness and functional intrinsic networks.

fields. These graded patterns of dynamic coupling reflect the topological and geometric embedding of these "middle hierarchy" regions.

Our results build on recent work showing that structure-function coupling is not uniform across the brain, but highly region-specific [8, 59, 79, 82]. These studies have consistently demonstrated that structure-function coupling is graded, with strong coupling in unimodal cortex and weak coupling in transmodal cortex. By applying a temporal unwrapping method to estimate functional co-fluctuation patterns from moment-to-moment, we show that structure-function coupling is not only regionally heterogeneous, but also highly dynamic [30]. Namely, we find that variability in coupling follows an inverted-U shape relative to the unimodal-transmodal hierarchy: the extremes or "anchors" of the hierarchy display more stable structure-function coupling, while regions intermediate in the hierarchy display more sizable fluctuations.

Interestingly, the most dynamic fluctuations were observed in insular cortex and frontal eye fields. In concert with the anterior cingulate and dorsolateral prefrontal cortices, the insula forms the ventral attention or salience network, which supports the orienting of attention to behaviourally-relevant stimuli, including sensory and autonomic signals related to the internal milieu [3, 77]. By participating in a diverse set of interdigitated connections with multiple brain regions, the insula is thought to dynamically coordinate communication among multiple cognitive systems [32, 43, 75]. In particular, the posterior portion of the insula displays prominent functional connectivity with sensory regions, while the anterior portion is primarily connected with frontal areas involved in higher cognitive function [61, 75]. In a similar vein, the frontal eye fields constitute a key node in the dorsal attention network, involved in biasing attention towards top-down goals and information foraging [15, 16].

Aligning these two findings, we observe a common functional theme of regions on the inteface between higher-order hetermodal cognition and primary perceptual and internal states. We speculate that the greater variability in local structure-function coupling in the insula and frontal eye fields delineates a potential mechanism by which signals are flexibly routed through these unique cortical hubs across wide domains. These "middle hierarchy" regions must engage in particularly broad coordination patterns, integrating ongoing unimodal information processing with the more sustained and extended operations in heteromodal cortex. This information is likely weighted by salience and goal relevance, while also allowing novel ongoing sensory information to gain access to heteromodal cortex.

The graded nature of local structure-function coupling appears to be shaped by the geometric embedding of individual brain regions. Namely, we also find an inverted-U shape relationship between connectivity distance and variability in structure-function coupling, such that regions with very short or very long connec-

tivity distance tend to display stable coupling, while regions with intermediate connectivity distance, particularly insular cortex and frontal eye fields, display more variable structure-function coupling. These findings resonate with a growing appreciation for how geometric relationships shape topological relationships in the brain [9, 11, 24, 53, 60, 67, 72]. In particular, physical separation from sensorimotor cortex is thought to correspond to graded variation in connectivity distance, culminating in predominantly long-range functional connectivity in association cortex [12, 44, 48, 54, 55]. The particular distribution of connection lengths that "middle hierarchy" regions participate in – leaning neither toward overly short- or long-range connectivity – may support flexible reconfiguration and participation in multiple systems [15, 32, 43, 75, 77], manifesting as variable structure-function coupling.

Our results build on a rapidly-developing literature on local structure-function relationships [73]. While traditional studies have focused on global structure-function relationships captured by a single forward model [33, 37, 38, 51, 52], numerous recent reports point to region-specific structure-function coupling patterns [8, 59, 79]. These structure-function relationships undergo extensive maturation and lifespan trajectories [8, 25]. Interestingly, regional differences in structure-function coupling are correlated with micro-architectural variations, including intracortical myelin and cellular composition [8, 79]. This suggests that local circuit properties — invisible to macroscale connectivity reconstructions — may additionally drive structure-function coupling [12]. Consistent with this notion, multiple modeling studies have recently shown that biophysical models constrained by regionally heterogeneous micro-architectural information, such as myelination, gene expression and neurotransmitter receptor profiles, make more accurate predictions about functional connectivity compared to regionally homogeneous models [20, 21, 82]. How regional differences in micro-architecture shape moment-to-moment fluctuations in structure-function coupling remains an important question for future research.

The present results need to be interpreted with respect to multiple limitations. First, structural connectivity networks were reconstructed using diffusion weighted MRI, a method that is susceptible to systematic false positives and negatives [18, 41, 47, 74]. Although the present findings are observed in individual participants and can be demonstrated using alternative methods, further development in computational tractometry is necessary. Likewise, it is important to note that there exist multiple alternative methods to quantify dynamic functional connectivity. We applied a recently-developed temporal unwrapping method that has been demonstrated to be robust to a wide range of methodological choices, including parcellation and global signal regression method, and are sensitive to individual differences [26, 28].

Collectively, the present work identifies patterns of local structure-function coupling that are systematically or-

ganized across the cortex and highly dynamic. The temporal tethering of structure and function points towards a rich and under-explored feature of the brain that may potentially help to understand how functions and cognitive processes are flexibly implemented and deployed.

## METHODS

### Data acquistion

Structural and functional data were obtained from the Human Connectome Project (s900 release [78]). Scans from 327 healthy young participants (age range 22-35 years) with no familial relationships were used, including individual measures of diffusion MRI and four resting-state functional MRI time-series (two scans on day one and two scans on day two, each of 15 minutes long). Data were processed following the procedure described in [57, 68].

#### *Structural network reconstruction*

Gray matter was parcellated into 400 cortical regions according to the Schaefer functional atlas [63]. Structural connectivity between regions was estimated for each participant using deterministic streamline tractography. First, the distribution of fiber orientation for each region was generated using the multi-shell multi-tissue constrained spherical deconvolution algorithm from the MRtrix3 package [22, 76] (https://www.mrtrix.org/). After that, the structural connectivity weight between any two regions was given by the number of streamlines normalized by the mean length of streamlines and the mean surface area of the two regions. This normalization reduces bias towards long fibers during streamline reconstruction, as well as the bias from differences in region sizes.

#### *Functional time-series reconstruction*

Functional MRI data were corrected for gradient nonlinearity, head motion (using a rigid body transformation), and geometric distortions (using scan pairs with opposite phase encoding directions (R/L, L/R) [19]). BOLD time-series were then subjected to a high-pass filter (>2000s FWHM) to correct for scanner drifts, and to the ICA-FIX process to remove additional noise [62]. The data was parcellated in the same atlas used for structural networks.

### Time-resolved structure-function coupling

To estimate region- and time-resolved structure-function coupling, we first constructed temporal co-fluctuation matrices. We started by calculating the element-wise product of the z-scored BOLD time-series

between pairs of brain regions [28]. Region pairs with an activity on the same side of the baseline will have a positive co-fluctuation value, whereas two regions that fluctuate in opposite directions at the same time will have a negative co-fluctuation value (Fig. 1a). The average across time of these co-fluctuation matrices recovers the Pearson correlation coefficient that is often used to define functional connectivity.

To define region-specific structure-function coupling, we constructed a multilinear regression model to predict the co-fluctuation profile of a node $i$ from its geometric and structural connectivity profile to all other nodes $j \neq i$ [79]. Predictors included shortest path length, communicability and Euclidean distance. We used the minimax-normalized weighted structural connectivity matrix for each individual, and calculated the metrics using the Python version of the Brain Connectivity Toolbox (https://github.com/fiuneuro/brainconn). A negative log transformation was applied to the structural connectivity weights before calculating the shortest path length [4].

Concretely, for region $i$, subject $s$, time point $t$, we have,

$$cofluc_{s,t,i} = \beta_0 + \beta_1 dist_i + \beta_2 spl_{s,i} + \beta_3 cmc_{s,i} \quad (1)$$

where $cofluc_{s,t,i}$ is the co-fluctuation profile, predicted by Euclidean distance $dist_i$, shortest path length $spl_{s,i}$, and weighted communicability $cmc_{s,i}$. The regression coefficients $\{\beta_0, \beta_1, \beta_2, \beta_3\}$ were estimated by ordinary least squares. Coupling was measured using adjusted R-squared $R_{i,t}^2$, a metric for goodness of fit. The regression was applied for individual profiles of brain regions, generating a cortical map of coupling values at each time point for each subject.

### Static and dynamic structure-function coupling

The multilinear regression model, when applied without temporal expansion, generates one $R^2$ value per brain region, which we refer to here as *static* coupling [79]. By incorporating temporal co-fluctuation patterns, we obtained structure-function coupling measure $R_t^2$ per region as a frame-by-frame time-series, which we call *dynamic* coupling. To assess how dynamic coupling differs from static coupling, we frame the question as comparing a single observation (static) with a distribution (dynamic). We defined three summary statistics: (1) the probability of having a larger dynamic coupling value compared to the static coupling, (2) the bias, and (3) the variance of the dynamic coupling to reproduce the static values. Bias was used to evaluate how dynamic values deviate from the static value. It was calculated as the median of the difference between the dynamic coupling values and the static coupling. Small values of bias indicate that dynamic coupling values are close to the static coupling values, while large values indicate deviation. Variance was used to evaluate the extent of scattering of the dynamic values. It was calculated as the standard

deviation of the distribution formed by the dynamic values. More specifically, we used the difference between the $84^{th}$ percentile and the $16^{th}$ percentile to avoid an underestimation for skewed distributions. Thus a low variance value means that the distribution had low variability, and high variance value indicates the opposite.

### Cortical annotations

Patterns of dynamic local structure-function coupling were contextualized relative to three common annotations: (1) 7 intrinsic functional networks as defined by Yeo et al. in [83], 7 cytoarchitectonic classes described by von Economo and Koskinas in [64, 81], and 10 functional hierarchy groups as defined in [79], based on the principal functional gradient reported by Margulies et al.. Collectively, these three partitions of the brain are thought to reflect multimodal hierarchies [39].

### Null models

To assess correspondence between coupling maps and cortical annotations, we applied spatial autocorrelation-preserving permutation tests, termed "spin tests" [1, 49, 79]. In this model, the cortical surface is projected to a sphere using the coordinates of the vertex closest to the center of mass of each parcel. The sphere is then randomly rotated, generating surface maps with randomized topography, where each parcel has a re-assigned value. The parcels corresponding to the medial wall were assigned to the closest rotated parcel [36, 69, 79]. The rotation was applied to one hemisphere and then mirrored to the other hemisphere. We generated 10000 spin permutations using *netneurotools* (https://github.com/netneurolab/netneurotools). Details of spatially-constrained null models in neuroimaging (https://github.com/netneurolab/markello_spatialnulls) were described in [49].

### ACKNOWLEDGMENTS

[1] Alexander-Bloch, A. F., Shou, H., Liu, S., Satterthwaite, T. D., Glahn, D. C., Shinohara, R. T., Vandekar, S. N., and Raznahan, A. (2018). On testing for spatial correspondence between maps of human brain structure and function. *Neuroimage*, 178:540–551.

[2] Allen, E. A., Damaraju, E., Plis, S. M., Erhardt, E. B., Eichele, T., and Calhoun, V. D. (2014). Tracking whole-brain connectivity dynamics in the resting state. *Cerebral cortex*, 24(3):663–676.

[3] Allen, M. (2020). Unravelling the neurobiology of interoceptive inference. *Trends Cogn Sci*, 24(4):265–266.

[4] Avena-Koenigsberger, A., Mišić, B., Hawkins, R. X., Griffa, A., Hagmann, P., Goñi, J., and Sporns, O. (2017). Path ensembles and a tradeoff between communication efficiency and resilience in the human connectome. *Brain Struct Funct*, 222(1):603–618.

[5] Avena-Koenigsberger, A., Misic, B., and Sporns, O. (2018). Communication dynamics in complex brain networks. *Nature Reviews Neuroscience*, 19(1):17.

[6] Azen, R. and Budescu, D. V. (2003). The dominance analysis approach for comparing predictors in multiple regression. *Psychological Methods*, 8(2):129–148.

[7] Battaglia, D., Boudou, T., Hansen, E. C. A., Lombardo, D., Chettouf, S., Daffertshofer, A., McIntosh, A. R., Zimmermann, J., Ritter, P., and Jirsa, V. (2020). Dynamic Functional Connectivity between order and randomness and its evolution across the human adult lifespan. *NeuroImage*, 222:117156.

[8] Baum, G. L., Cui, Z., Roalf, D. R., Ciric, R., Betzel, R. F., Larsen, B., Cieslak, M., Cook, P. A., Xia, C. H., Moore, T. M., et al. (2020). Development of structure–function coupling in human brain networks during youth. *Proceedings of the National Academy of Sciences*, 117(1):771–778.

[9] Betzel, R. F., Avena-Koenigsberger, A., Goñi, J., He, Y., De Reus, M. A., Griffa, A., Vértes, P. E., Mišic, B., Thiran, J.-P., Hagmann, P., et al. (2016a). Generative models of the human connectome. *NeuroImage*, 124:1054–1064.

[10] Betzel, R. F., Fukushima, M., He, Y., Zuo, X.-N., and Sporns, O. (2016b). Dynamic fluctuations coincide with periods of high and low modularity in resting-state functional brain networks. *NeuroImage*, 127:287–297.

[11] Betzel, R. F., Griffa, A., Hagmann, P., and Mišić, B. (2019). Distance-dependent consensus thresholds for generating group-representative structural brain networks. *Net Neurosci*, 3(2):475–496.

[12] Buckner, R. L. and Krienen, F. M. (2013). The evolution of distributed association networks in the human brain. *Trends in cognitive sciences*, 17(12):648–665.

[13] Budescu, D. V. (1993). Dominance analysis: A new approach to the problem of relative importance of predictors in multiple regression. *Psychological Bulletin*, 114(3):542–551.

[14] Chang, C. and Glover, G. H. (2010). Time–frequency dynamics of resting-state brain connectivity measured with fMRI. *NeuroImage*, 50(1):81–98.

[15] Corbetta, M., Patel, G., and Shulman, G. L. (2008). The reorienting system of the human brain: from environment to theory of mind. *Neuron*, 58(3):306–324.

[16] Corbetta, M. and Shulman, G. L. (2002). Control of goal-directed and stimulus-driven attention in the brain. *Nat Rev Neurosci*, 3(3):201–215.

[17] Crofts, J. J. and Higham, D. J. (2009). A weighted communicability measure applied to complex brain networks. *Journal of the Royal Society Interface*, 6(33):411–414.

[18] de Reus, M. A. and van den Heuvel, M. P. (2013). Estimating false positives and negatives in brain networks. *NeuroImage*, 70:402–409.

[19] de Wael, R. V., Larivière, S., Caldairou, B., Hong, S.-J., Margulies, D. S., Jefferies, E., Bernasconi, A., Smallwood, J., Bernasconi, N., and Bernhardt, B. C. (2018). Anatomical and microstructural determinants of hippocampal subfield functional connectome embedding. *Proceedings of the National Academy of Sciences*, 115(40):10154–10159.

[20] Deco, G., Aquino, K., Arnatkevičiūtė, A., Oldham, S., Sabaroedin, K., Rogasch, N. C., Kringelbach, M. L., and Fornito, A. (2020). Dynamical consequences of regional heterogeneity in the brain's transcriptional landscape. *bioRxiv*, page 2020.10.28.359943.

[21] Demirtaş, M., Burt, J. B., Helmer, M., Ji, J. L., Adkinson, B. D., Glasser, M. F., Van Essen, D. C., Sotiropoulos, S. N., Anticevic, A., and Murray, J. D. (2019). Hierarchical heterogeneity across human cortex shapes large-scale neural dynamics. *Neuron*, 101(6):1181–1194.

[22] Dhollander, T., Raffelt, D., and Connelly, A. (2016). Unsupervised 3-tissue response function estimation from single-shell or multi-shell diffusion mr data without a co-registered t1 image. In *ISMRM Workshop on Breaking the Barriers of Diffusion MRI*, volume 5, page 5.

[23] Eichenbaum, A., Pappas, I., Lurie, D., Cohen, J. R., and D'Esposito, M. (2021). Differential contributions of static and time-varying functional connectivity to human behavior. *Network Neuroscience*, 5(1):145–165.

[24] Ercsey-Ravasz, M., Markov, N. T., Lamy, C., Van Essen, D. C., Knoblauch, K., Toroczkai, Z., and Kennedy, H. (2013). A predictive network model of cerebral cortical connectivity based on a distance rule. *Neuron*, 80(1):184–197.

[25] Esfahlani, F. Z., Faskowitz, J., Slack, J., Misic, B., and Betzel, R. (2021). Local structure-function relationships in human brain networks across the human lifespan. *bioRxiv*.

[26] Esfahlani, F. Z., Jo, Y., Faskowitz, J., Byrge, L., Kennedy, D. P., Sporns, O., and Betzel, R. F. (2020). High-amplitude cofluctuations in cortical activity drive functional connectivity. *Proceedings of the National Academy of Sciences*, 117(45):28393–28401.

[27] Estrada, E. and Hatano, N. (2008). Communicability in complex networks. *Physical Review E*, 77(3):036111.

[28] Faskowitz, J., Esfahlani, F. Z., Jo, Y., Sporns, O., and Betzel, R. F. (2020). Edge-centric functional network representations of human cerebral cortex reveal overlapping system-level architecture. *Nature neuroscience*, 23(12):1644–1654.

[29] Fornito, A., Zalesky, A., and Bullmore, E. (2016). *Fundamentals of Brain Network Analysis*. Academic Press.

[30] Fukushima, M., Betzel, R. F., He, Y., van den Heuvel, M. P., Zuo, X.-N., and Sporns, O. (2018). Structure–function relationships during segregated and integrated network states of human brain functional connectivity. *Brain Structure and Function*, 223(3):1091–1106.

[31] Fukushima, M. and Sporns, O. (2020). Structural determinants of dynamic fluctuations between segregation and integration on the human connectome. *Communications Biology*, 3(1):1–11.

[32] Ghaziri, J., Tucholka, A., Girard, G., Houde, J.-C., Boucher, O., Gilbert, G., Descoteaux, M., Lippé, S., Rainville, P., and Nguyen, D. K. (2017). The corticocortical structural connectivity of the human insula. *Cereb Cortex*, 27(2):1216–1228.

[33] Goñi, J., Van Den Heuvel, M. P., Avena-Koenigsberger, A., De Mendizabal, N. V., Betzel, R. F., Griffa, A., Hagmann, P., Corominas-Murtra, B., Thiran, J.-P., and Sporns, O. (2014). Resting-brain functional connectivity predicted by analytic measures of network communication. *Proceedings of the National Academy of Sciences*, 111(2):833–838.

[34] Gonzalez-Castillo, J., Hoy, C. W., Handwerker, D. A., Robinson, M. E., Buchanan, L. C., Saad, Z. S., and Bandettini, P. A. (2015). Tracking ongoing cognition in individuals using brief, whole-brain functional connectivity patterns. *Proceedings of the National Academy of Sciences*, 112(28):8762–8767.

[35] Gu, Z., Jamison, K. W., Sabuncu, M. R., and Kuceyeski, A. (2020). Regional structural-functional connectome coupling is heritable and associated with age, sex and cognition in adults. *bioRxiv*.

[36] Hansen, J. Y., Markello, R. D., Vogel, J. W., Seidlitz, J., Bzdok, D., and Misic, B. (2021). Mapping gene transcription and neurocognition across human neocortex. *Nature Human Behaviour*, pages 1–11.

[37] Honey, C. J., Kötter, R., Breakspear, M., and Sporns, O. (2007). Network structure of cerebral cortex shapes functional connectivity on multiple time scales. *Proc Natl Acad Sci USA*, 104(24):10240–10245.

[38] Honey, C. J., Sporns, O., Cammoun, L., Gigandet, X., Thiran, J.-P., Meuli, R., and Hagmann, P. (2009). Predicting human resting-state functional connectivity from structural connectivity. *Proc Natl Acad Sci USA*, 106(6):2035–2040.

[39] Huntenburg, J. M., Bazin, P.-L., and Margulies, D. S. (2018). Large-scale gradients in human cortical organization. *Trends Cogn Sci*, 22(1):21–31.

[40] Jo, Y., Faskowitz, J., Esfahlani, F. Z., Sporns, O., and Betzel, R. F. (2020). Subject identification using edge-centric functional connectivity. *bioRxiv*.

[41] Jones, D. K., Knösche, T. R., and Turner, R. (2013). White matter integrity, fiber count, and other fallacies: the do's and don'ts of diffusion mri. *NeuroImage*, 73:239–254.

[42] Kong, X., Kong, R., Orban, C., Peng, W., Zhang, S., Anderson, K., Holmes, A., Murray, J. D., Deco, G., van den Heuvel, M., et al. (2021). Anatomical and functional gradients shape dynamic functional connectivity in the human brain. *bioRxiv*.

[43] Kurth, F., Zilles, K., Fox, P. T., Laird, A. R., and Eickhoff, S. B. (2010). A link between the systems: functional differentiation and integration within the human insula revealed by meta-analysis. *Brain Struct Funct*, 214(5-6):519–534.

[44] Larivière, S., Weng, Y., Vos de Wael, R., Royer, J., Frauscher, B., Wang, Z., Bernasconi, A., Bernasconi, N., Schrader, D. V., Zhang, Z., et al. (2020). Functional connectome contractions in temporal lobe epilepsy: Microstructural underpinnings and predictors of surgical outcome. *Epilepsia*, 61(6):1221–1233.

[45] Liégeois, R., Laumann, T. O., Snyder, A. Z., Zhou, J., and Yeo, B. T. T. (2017). Interpreting temporal fluctuations in resting-state functional connectivity MRI. *NeuroImage*, 163:437–455.

[46] Lurie, D. J., Kessler, D., Bassett, D. S., Betzel, R. F., Breakspear, M., Kheilholz, S., Kucyi, A., Liégeois, R., Lindquist, M. A., McIntosh, A. R., Poldrack, R. A., Shine, J. M., Thompson, W. H., Bielczyk, N. Z., Douw, L., Kraft, D., Miller, R. L., Muthuraman, M., Pasquini, L., Razi, A., Vidaurre, D., Xie, H., and Calhoun, V. D. (2020). Questions and controversies in the study of time-varying functional connectivity in resting fMRI. *Network Neuroscience*, 4(1):30–69.

[47] Maier-Hein, K. H., Neher, P. F., Houde, J.-C., Côté, M.-A., Garyfallidis, E., Zhong, J., Chamberland, M., Yeh, F.-C., Lin, Y.-C., Ji, Q., et al. (2017). The challenge of mapping the human connectome based on diffusion tractography. *Nat Commun*, 8(1):1–13.

[48] Margulies, D. S., Ghosh, S. S., Goulas, A., Falkiewicz, M., Huntenburg, J. M., Langs, G., Bezgin, G., Eickhoff, S. B., Castellanos, F. X., Petrides, M., et al. (2016). Situating the default-mode network along a principal gradient of macroscale cortical organization. *Proceedings of the National Academy of Sciences*, 113(44):12574–12579.

[49] Markello, R. D. and Misic, B. (2021). Comparing spatial null models for brain maps. *NeuroImage*, page 118052.

[50] Mesulam, M.-M. (1998). From sensation to cognition. *Brain: a journal of neurology*, 121(6):1013–1052.

[51] Mišić, B., Betzel, R. F., De Reus, M. A., Van Den Heuvel, M. P., Berman, M. G., McIntosh, A. R., and Sporns, O. (2016). Network-level structure-function relationships in human neocortex. *Cereb Cortex*, 26(7):3285–3296.

[52] Mišić, B., Betzel, R. F., Nematzadeh, A., Goni, J., Griffa, A., Hagmann, P., Flammini, A., Ahn, Y.-Y., and Sporns, O. (2015). Cooperative and competitive spreading dynamics on the human connectome. *Neuron*, 86(6):1518–1529.

[53] Mišić, B., Fatima, Z., Askren, M. K., Buschkuehl, M., Churchill, N., Cimprich, B., Deldin, P. J., Jaeggi, S., Jung, M., Korostil, M., et al. (2014). The functional connectivity landscape of the human brain. *PLoS One*, 9(10):e111007.

[54] Oligschläger, S., Huntenburg, J. M., Golchert, J., Lauckner, M. E., Bonnen, T., and Margulies, D. S. (2017). Gradients of connectivity distance are anchored in primary cortex. *Brain Struct Funct*, 222(5):2173–2182.

[55] Oligschläger, S., Xu, T., Baczkowski, B. M., Falkiewicz, M., Falchier, A., Linn, G., and Margulies, D. S. (2019). Gradients of connectivity distance in the cerebral cortex of the macaque monkey. *Brain Struct Funct*, 224(2):925–935.

[56] Paquola, C., De Wael, R. V., Wagstyl, K., Bethlehem, R. A., Hong, S.-J., Seidlitz, J., Bullmore, E. T., Evans, A. C., Misic, B., Margulies, D. S., et al. (2019). Microstructural and functional gradients are increasingly dissociated in transmodal cortices. *PLoS biology*, 17(5):e3000284.

[57] Park, B.-y., Vos de Wael, R., Paquola, C., Larivière, S., Benkarim, O., Royer, J., Tavakol, S., Cruces, R. R., Li, Q., Valk, S. L., Margulies, D. S., Mišić, B., Bzdok, D., Smallwood, J., and Bernhardt, B. C. (2021). Signal diffusion along connectome gradients and inter-hub routing differentially contribute to dynamic human brain function. *NeuroImage*, 224:117429.

[58] Preti, M. G., Bolton, T. A., and Van De Ville, D. (2017). The dynamic functional connectome: State-of-the-art and perspectives. *NeuroImage*, 160:41–54.

[59] Preti, M. G. and Van De Ville, D. (2019). Decoupling of brain function from structure reveals regional behavioral specialization in humans. *Nature communications*, 10(1):1–7.

[60] Roberts, J. A., Perry, A., Lord, A. R., Roberts, G., Mitchell, P. B., Smith, R. E., Calamante, F., and Breakspear, M. (2016). The contribution of geometry to the human connectome. *NeuroImage*, 124:379–393.

[61] Royer, J., Paquola, C., Larivière, S., de Wael, R. V., Tavakol, S., Lowe, A. J., Benkarim, O., Evans, A. C., Bzdok, D., Smallwood, J., et al. (2020). Myeloarchitecture gradients in the human insula: Histological underpinnings and association to intrinsic functional connectivity. *NeuroImage*, 216:116859.

[62] Salimi-Khorshidi, G., Douaud, G., Beckmann, C. F., Glasser, M. F., Griffanti, L., and Smith, S. M. (2014). Automatic denoising of functional mri data: combining independent component analysis and hierarchical fusion of classifiers. *Neuroimage*, 90:449–468.

[63] Schaefer, A., Kong, R., Gordon, E. M., Laumann, T. O., Zuo, X.-N., Holmes, A. J., Eickhoff, S. B., and Yeo, B. T. (2018). Local-global parcellation of the human cerebral cortex from intrinsic functional connectivity mri. *Cerebral cortex*, 28(9):3095–3114.

[64] Scholtens, L. H., de Reus, M. A., de Lange, S. C., Schmidt, R., and van den Heuvel, M. P. (2018). An mri von economo–koskinas atlas. *Neuroimage*, 170:249–256.

[65] Seguin, C., Tian, Y., and Zalesky, A. (2020). Network communication models improve the behavioral and functional predictive utility of the human structural connectome. *Network Neuroscience*, 4(4):980–1006.

[66] Seguin, C., Van Den Heuvel, M. P., and Zalesky, A. (2018). Navigation of brain networks. *Proceedings of the National Academy of Sciences*, 115(24):6297–6302.

[67] Sepulcre, J., Liu, H., Talukdar, T., Martincorena, I., Yeo, B. T., and Buckner, R. L. (2010). The organization of local and distant functional connectivity in the human brain. *PLoS Comput Biol*, 6(6):e1000808.

[68] Shafiei, G., Markello, R. D., De Wael, R. V., Bernhardt, B. C., Fulcher, B. D., and Misic, B. (2020a). Topographic gradients of intrinsic dynamics across neocortex. *Elife*, 9:e62116.

[69] Shafiei, G., Markello, R. D., Makowski, C., Talpalaru, A., Kirschner, M., Devenyi, G. A., Guma, E., Hagmann, P., Cashman, N. R., Lepage, M., et al. (2020b). Spatial patterning of tissue volume loss in schizophrenia reflects brain network architecture. *Biol Psychiat*, 87(8):727–735.

[70] Shine, J. M., Bissett, P. G., Bell, P. T., Koyejo, O., Balsters, J. H., Gorgolewski, K. J., Moodie, C. A., and Poldrack, R. A. (2016). The Dynamics of Functional Brain Networks: Integrated Network States during Cognitive Task Performance. *Neuron*, 92(2):544–554.

[71] Shine, J. M. and Poldrack, R. A. (2018). Principles of dynamic network reconfiguration across diverse brain states. *NeuroImage*, 180:396–405.

[72] Stiso, J. and Bassett, D. S. (2018). Spatial embedding imposes constraints on neuronal network architectures. *Trends Cogn Sci*, 22(12):1127–1142.

[73] Suárez, L. E., Markello, R. D., Betzel, R. F., and Misic, B. (2020). Linking Structure and Function in Macroscale Brain Networks. *Trends in Cognitive Sciences*.

[74] Thomas, C., Frank, Q. Y., Irfanoglu, M. O., Modi, P., Saleem, K. S., Leopold, D. A., and Pierpaoli, C. (2014). Anatomical accuracy of brain connections derived from diffusion mri tractography is inherently limited. *Proc Natl Acad Sci USA*, 111(46):16574–16579.

[75] Tian, Y. and Zalesky, A. (2018). Characterizing the functional connectivity diversity of the insula cortex: Sub-

regions, diversity curves and behavior. *NeuroImage*, 183:716–733.

[76] Tournier, J.-D., Smith, R., Raffelt, D., Tabbara, R., Dhollander, T., Pietsch, M., Christiaens, D., Jeurissen, B., Yeh, C.-H., and Connelly, A. (2019). Mrtrix3: A fast, flexible and open software framework for medical image processing and visualisation. *NeuroImage*, 202:116137.

[77] Uddin, L. Q. (2015). Salience processing and insular cortical function and dysfunction. *Nat Rev Neurosci*, 16(1):55–61.

[78] Van Essen, D. C., Ugurbil, K., Auerbach, E., Barch, D., Behrens, T. E., Bucholz, R., Chang, A., Chen, L., Corbetta, M., Curtiss, S. W., et al. (2012). The human connectome project: a data acquisition perspective. *Neuroimage*, 62(4):2222–2231.

[79] Vázquez-Rodríguez, B., Suárez, L. E., Markello, R. D., Shafiei, G., Paquola, C., Hagmann, P., Van Den Heuvel, M. P., Bernhardt, B. C., Spreng, R. N., and Misic, B. (2019). Gradients of structure–function tethering across neocortex. *Proceedings of the National Academy of Sciences*, 116(42):21219–21227.

[80] Vidaurre, D., Smith, S. M., and Woolrich, M. W. (2017). Brain network dynamics are hierarchically organized in time. *Proceedings of the National Academy of Sciences*, 114(48):12827–12832.

[81] von Economo, C. F. and Koskinas, G. N. (1925). *Die cytoarchitektonik der hirnrinde des erwachsenen menschen*. J. Springer.

[82] Wang, P., Kong, R., Kong, X., Liégeois, R., Orban, C., Deco, G., Van Den Heuvel, M. P., and Yeo, B. T. (2019). Inversion of a large-scale circuit model reveals a cortical hierarchy in the dynamic resting human brain. *Science advances*, 5(1):eaat7854.

[83] Yeo, B. T., Krienen, F. M., Sepulcre, J., Sabuncu, M. R., Lashkari, D., Hollinshead, M., Roffman, J. L., Smoller, J. W., Zöllei, L., Polimeni, J. R., et al. (2011). The organization of the human cerebral cortex estimated by intrinsic functional connectivity. *Journal of neurophysiology*.

[84] Zalesky, A., Fornito, A., Cocchi, L., Gollo, L. L., and Breakspear, M. (2014). Time-resolved resting-state brain networks. *Proc Natl Acad Sci USA*, 111(28):10341–10346.
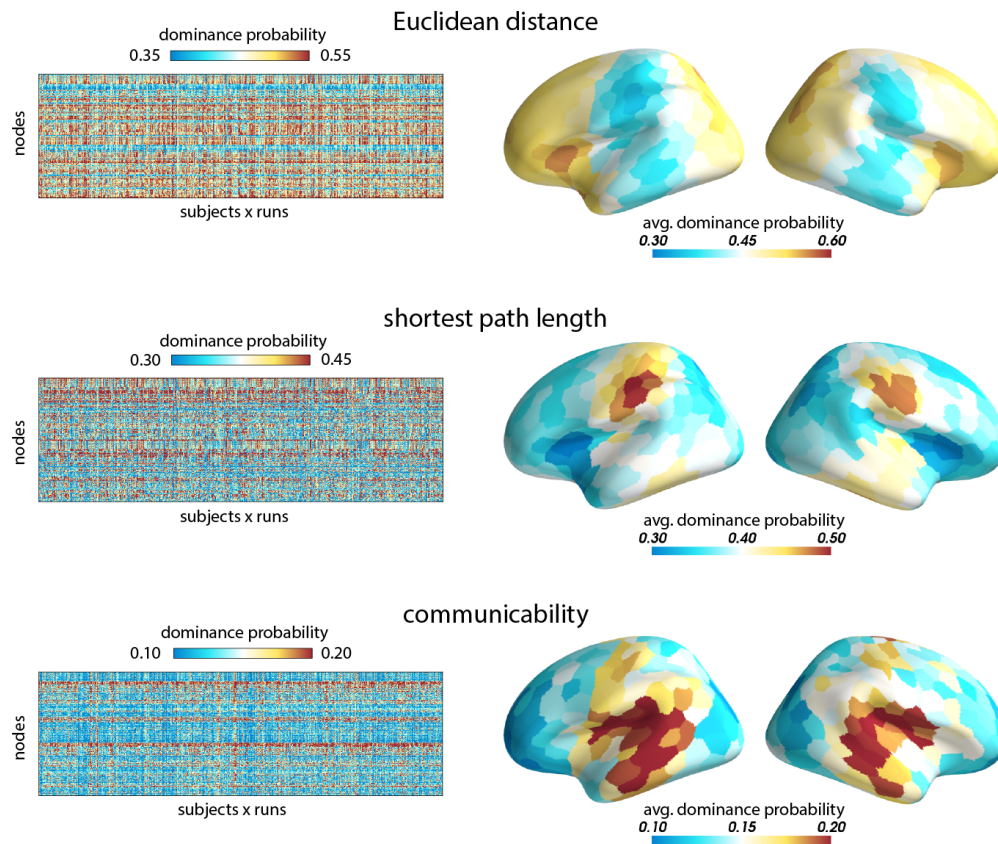
**Figure S1 | Predictor contributions.** Dominance Analysis was used to quantify the distinct contributions of the three predictors in the mulitlinear model (Euclidean distance, path length and communicability) [6, 13] (https://github.com/dominance-analysis/dominance-analysis). The technique estimates the relative importance of predictors by constructing all possible combinations of predictors and quantifying the relative contribution of each predictor as additional variance explained (i.e. gain in $R^2$) by adding that predictor to the models. The incremental $R^2$ contribution of each predictor to a given subset model of all the other predictors is then calculated as the increase in $R^2$ due to the addition of that predictor to the regression model. Left: dominance over time for the three predictors. Each column in the matrix shows the frequency of the predictor being the dominant predictor through time. Right: brain map of the matrix averaged over subjects and runs.
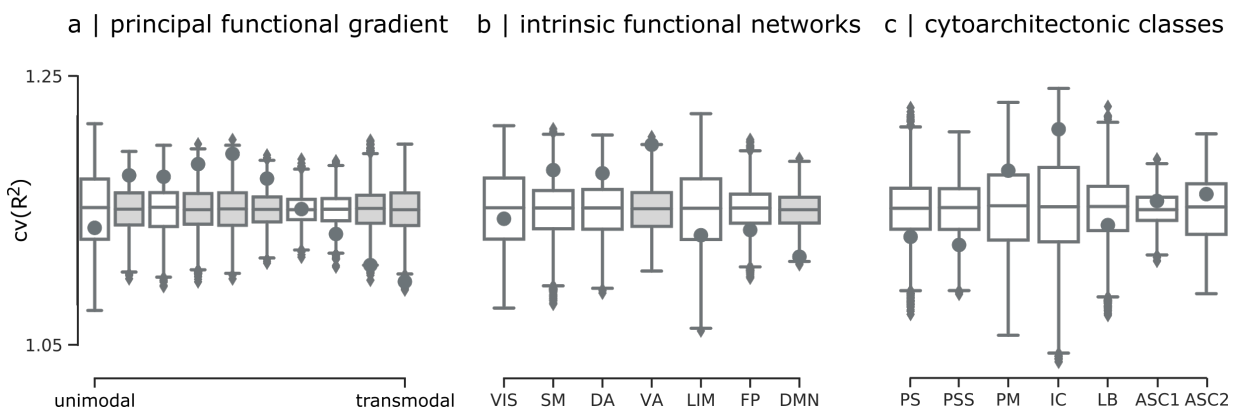


**Figure S2 | Spin test of the coefficient of variation of the structure-function coupling.** Black points show partition-specific mean $\mathrm{cv}(R^2)$ (same as results in Fig. 3c-e). Boxplots show distributions of partition-specific mean $\mathrm{cv}(R^2)$ for 10,000 spatial autocorrelation-preserving null models ("spin tests") [1, 49]. Darker (filled) and lighter (non-filled) boxes show partitions for which $\mathrm{cv}(R^2)$ is statistically significant ($p < 0.05$) and non-significant ($p > 0.05$), respectively.
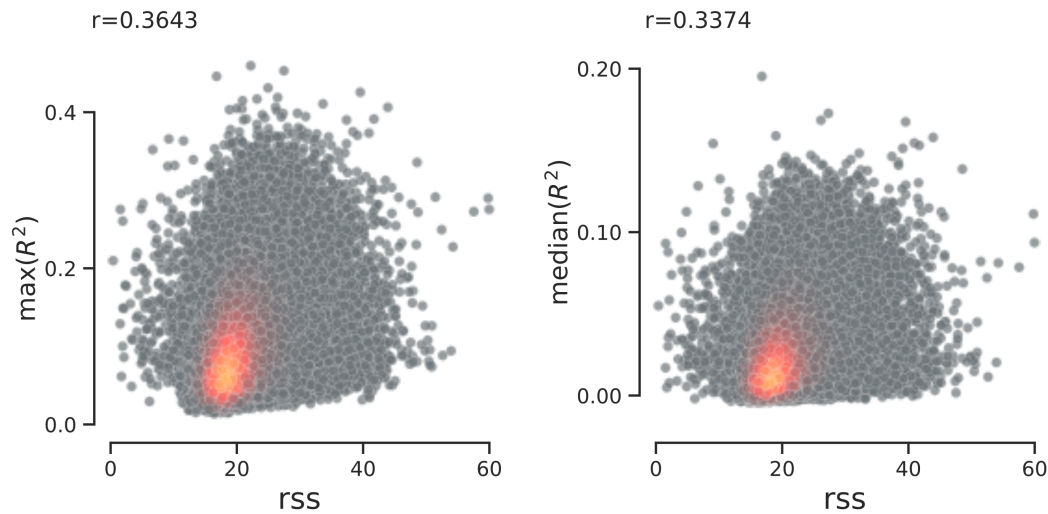
Figure S3 | **Co-fluctuation amplitude and structure-function coupling** To characterize the amplitude of the co-fluctuation time series, Esfahlani et al. calculated the root sum square (RSS) of the co-fluctuation time series across the network at each time point. The maximum and median of each of the $R_t^2$ vectors (column vector at figure 1c) is positively correlated with the RSS.